sustainability

MDPI

Article

Fabrication of Sustainable Sodium Alginate/Polyethyleneimine/Polyvinyl Alcohol Multilayer Composite Electrospun Nanofiber Membrane for Efficient Cu^{2+} Removal

Boshi Xie, Ziao Zhang, Yujie Lu, Lijuan Cui, Chao Xu, Weijian Shi and Shuping Wu *

Institute of Polymer Materials, School of Materials Science & Engineering, Jiangsu University, Zhenjiang 212013, China; 3210708108@stmail.ujs.edu.cn (B.X.); 3220708134@stmail.ujs.edu.cn (Z.Z.); 3220708089@stmail.ujs.edu.cn (Y.L.); 2222305061@stmail.ujs.edu.cn (L.C.); 2212205008@stmail.ujs.edu.cn (C.X.); 2222105045@stmail.ujs.edu.cn (W.S.)

* Correspondence: shupingwu@ujs.edu.cn

Abstract: In pursuit of sustainable solutions for water pollution mitigation, we have successfully employed electrospinning technology to fabricate a multilayered sodium alginate (SA)/polyethyleneimine (PEI)/polyvinyl alcohol (PVA) nanocomposite fiber membrane, with a focus on enhancing its adsorption capacity for Cu^{2+} ions in wastewater. Our research underscores the potential of this novel membrane, characterized by its small diameter, high uniformity, and expansive surface area, in effectively filtering heavy metal ions. By optimizing critical electrospinning parameters such as a voltage of 19.5 KV, a collector distance of 8 cm, a specific mass ratio of SA:PEI: PVA (1:2:6), and an injection rate of 8 μL/min, we achieved a nanofiber membrane with an average diameter of 112.5 nm, exhibiting exceptional morphological characteristics and high efficiency. Notably, the membrane exhibited an adsorption capacity of over 85% for Cu^{2+} during initial testing, maintaining over 80% efficiency throughout four consecutive filtration cycles. This work not only advances the field of nanocomposite membranes for water purification but also contributes significantly to the broader goal of achieving environmental sustainability by mitigating the impact of heavy metal contamination in water bodies.

Keywords: biodegradable materials; wastewater treatment; electrospinning; heavy metal filtration; eco-friendly nanofibers; resource conservation

Citation: Xie, B.; Zhang, Z.; Lu, Y.; Cui, L.; Xu, C.; Shi, W.; Wu, S. Fabrication of Sustainable Sodium Alginate/Polyethyleneimine/Polyvinyl Alcohol Multilayer Composite Electrospun Nanofiber Membrane for Efficient Cu^{2+} Removal. *Sustainability* **2024**, *16*, 5993. https://doi.org/10.3390/su16145993

Academic Editors: Maria L. Auad and Agostina Chiavola

Received: 19 April 2024
Revised: 26 June 2024
Accepted: 12 July 2024
Published: 13 July 2024

1. Introduction

Water, essential for human life, is increasingly threatened by pollution, especially heavy metals stemming from industrialization and agriculture. These pollutants are toxic, non-biodegradable, and accumulate in the environment, posing risks to aquatic life and human health [1–4]. Membrane separation technology offers an efficient solution and is renowned for its energy efficiency, compact design, and high separation performance [5–9]. It selectively removes pollutants based on their properties, preserving water resources. Additionally, the sustainable synthesis of polymers through natural renewable resources has been extensively researched and is becoming an inevitable choice for the polymer industry [10–12]. Moreover, the utilization of natural and renewable resources for the synthesis of polymer nanomembrane materials holds immense potential. These materials not only enhance the sustainability of water treatment processes but also contribute to environmental protection.

Electrospinning, a pioneering technology that has revolutionized nanofiber material fabrication, continues to gain momentum due to its crucial role in the development of highly efficient adsorbent membranes. Lord Rayleigh's work in the late 19th century provided the theoretical underpinnings for this process, which utilizes electrically charged jets of polymer solutions or melts to generate ultrafine fibers. The importance of electrospinning lies in

its exceptional characteristics, such as ultra-high porosity, vast specific surface area, and uniformity in fiber diameter distribution, making it ideal for various membrane processing applications [11,13–17]. At the forefront of technological advancements, electrospinning has broadened its horizons to encompass diverse applications, including filtration and separation, composite reinforcement, tissue engineering, biocatalysis, and controlled drug release [18–23]. Recent developments have further enhanced the technique's capabilities, such as the introduction of new polymer systems and functionalization methods that allow for the precise control of nanofiber properties. This, in turn, has led to the development of membranes with unprecedented performance in areas like water purification, energy storage, and medical devices. The adaptability of electrospinning to a wide range of raw materials tailored to specific needs has made it an invaluable tool in the pursuit of innovative solutions for complex challenges.

Electrospun nanofibers have proven to be exceptional nanomaterials with significant potential for removing heavy metal ions. Yang et al. have developed a novel CS-PGMA-PEI electrospun membrane enriched with amino groups, which exhibits superior heavy metal ion removal from water. Characterization techniques confirm the integration of amino groups, and batch adsorption tests reveal optimal pH conditions and high adsorption capacities for Cr(VI), Cu(II), and Co(II). The membrane follows pseudo-second-order and Langmuir models, indicating monolayer adsorption, with a particular affinity for Cr(VI). Its renewability and stability suggest its potential as a sustainable water treatment membrane, advancing the field of water purification [24]. The CS-PGMA-PEI membrane rapidly reached adsorption equilibrium within 60 min, demonstrating maximum adsorption capacities for Cr(VI), Cu(II), and Co(II) at 138.96, 69.27, and 68.31 mg/g, respectively, according to the Langmuir model. This study highlights the membrane's potential for efficient water purification, showing notable reproducibility and stability in removing heavy metal ions. In our previous research, we developed carboxymethyl cellulose (CMC)/polyvinyl alcohol (PVA) composite nanofiber membranes through electrostatic spinning, utilizing CMC and PVA with glutaraldehyde as a crosslinker, and characterized them using techniques such as scanning electron microscopy (SEM), Fourier transform infrared spectrometry (FTIR), thermogravimetric analysis (TGA), ultraviolet spectroscopy (UV), and energy spectrum analysis. The optimized spinning parameters (23 KV and 2 μL/min) resulted in fibers with a reduced diameter of 183 nm, indicating finer and more uniformly distributed fibers. The membranes demonstrated high chemical adsorption efficiencies for Cu^{2+} and Cr^{6+}, with retention rates of 97.2% and 98.8%, respectively, and the adsorption capacities were 26.34 $mg{\cdot}g^{-1}$ for Cu^{2+} and 28.93 $medsg{\cdot}g^{-1}$ for Cr^{6+}, consistent with the pseudo-second-order kinetic model and the Langmuir isotherm. At the same time, our team successfully synthesized a chitosan (CS)/polyvinylpyrrolidone (PVP)/polyvinyl alcohol (PVA) hollow nanofiber membrane (CS/PVP/PVA-HNM) via coaxial electrospinning [21]. This membrane demonstrated remarkable permeability and adsorption separation. Specifically, the CS/PVP/PVA-HNM had a pure water permeability of 4367.02 $L{\cdot}m^{-2}{\cdot}h^{-1}{\cdot}bar^{-1}$. The hollow electrospun nanofibrous membrane exhibited a continuous interlaced nanofibrous framework structure with the extraordinary advantages of high porosity and high permeability. The rejection ratios of CS/PVP/PVA-HNM for Cu^{2+}, Ni^{2+}, Cd^{2+}, Pb^{2+}, malachite green (MG), methylene blue (MB), and crystal violet (CV) were 96.91%, 95.29%, 87.50%, 85.13%, 88.21%, 83.91%, and 71.99%, and the maximum adsorption capacities were 106.72, 97.46, 88.10, 87.81, 53.45, 41.43, and 30.97 $mg{\cdot}g^{-1}$, respectively. This work demonstrates a strategy for the synthesis of hollow nanofibers, which provides a novel concept for the design and fabrication of highly efficient adsorption and separation membranes.

Sodium alginate (SA), a natural polysaccharide extracted from various species of brown algae, including macroalgae and kelp, is a linear block copolymer consisting of β-D-mannuronic acid and α-L-glucuronic acid, with the molecular formula $(C_6H_7NaO_6)_n$. It is characterized by a high density of carboxyl (-COOH) and hydroxyl (-OH) functional groups along its molecular chain [25–27]. These groups enable sodium alginate to effectively bind with divalent or higher-valency metal ions M^{n+} ($n \geq 2$), facilitating the ion exchange pro-

cesses where H^+ and Na^+ are replaced, forming a complex three-dimensional gel network enriched with M^{n+}. This property makes sodium alginate an ideal candidate for use as an investment material in a variety of applications [28–32]. Sodium alginate is non-toxic, has excellent film-forming ability, has excellent biocompatibility and biodegradability, and is widely used in various industries. These include food production as thickeners and stabilizers; pharmaceuticals, for use in drug delivery systems; cosmetics, for their moisturizing properties; and the textile industry, especially in dyeing processes. Its versatility and environmental friendliness underscore its growing importance in sustainable industrial practices, reflecting a shift toward more environmentally friendly materials in technology and product development.

Polyethyleneimine (PEI), also known as polyazacyclopropane, is a water-soluble macromolecule with the highest known cationic charge density among organic polymers. PEI excels in water treatment applications due to its dense amine groups—primary, secondary, and tertiary [33–37]. These groups facilitate the binding of heavy metal ions in wastewater through mechanisms like ion exchange, electrostatic interactions, chelation, and coordination, leading to high adsorption capacity. PEI's effectiveness is highlighted in various studies, including those by Gao et al., who immobilized soluble PEI using polydopamine (PDA) polymerization, facilitating effective Pb^{2+} removal through a cooperative adsorption mechanism that leverages charged SO_3H groups within a polystyrene matrix and in situ PDA formation at room temperature [38]. This hybrid adsorbent demonstrated exceptional selectivity and efficiency, achieving rapid lead removal kinetics, excellent sorption–regeneration properties, and an outstanding capacity for treating Pb-contaminated water with potential applicability to other metals like Fe^{3+}, Cu^{2+}, and Ni^{2+}. For instance, Bucatariu et al. modified spherical silica microparticles with linear and branched poly(ethyleneimine) (PEI) chains through layer-by-layer deposition involving a copper complex and poly(acrylic acid), followed by selective crosslinking and removal of copper and PAA, to create functional silica/$(PEIL)_{10}$ and silica/$(PEIB)_{10}$ composites [39]. These composites demonstrated effective sorption of heavy metals like Cu^{2+}, Ni^{2+}, Co^{2+}, and Cd^{2+} in batch and column experiments under noncompetitive conditions. Additionally, Tofighy et al. developed a positively charged membrane using hyperbranched polyethyleneimine (HPEI) as a crosslinking agent through a vacuum filtration method, aimed at efficiently removing divalent heavy metal ions from contaminated water [40]. The resulting HPEI crosslinked membrane demonstrated excellent performance, highlighted by its ability to selectively reject heavy metal ions and maintain effectiveness over multiple regeneration cycles, indicating its potential for repeated use in water purification applications.

In this study, we aimed to fabricate multilayer composite nanofibrous membranes using three polymer raw materials: SA, PEI, and PVA. SA and PEI were chosen for their effective functional groups that facilitate Cu^{2+} adsorption, while PVA served as a co-spinning solution and carrier, enhancing the filament-forming properties essential for electrospinning. The spinning process involved the preparation of two hybrid spinning solutions, SA/PVA and PEI/PVA, which were alternately and cyclically spun using electrospinning to create nanofiber membranes with sufficient thickness for filtration. The resulting nanofiber membranes, theoretically insoluble in water, exhibited significant hydrogen bonding interactions within SA and PVA as well as between PEI and PVA, and interlayer hydrogen bonding between SA and PEI, enhancing the structural integrity. These multilayer membranes were subjected to both single and repeated Cu(II) filtration tests, with their performance and structural characteristics analyzed using SEM, energy dispersive spectroscopy (EDS), FTIR, UV-visible spectrophotometry (UV-vis), X-ray diffraction (XRD), and thermogravimetric analysis (TG). The objective of this study was to explore the feasibility and efficiency of using electrospun multilayer composite nanofibrous membranes for the adsorption and removal of Cu(II) from aqueous solutions.

2. Experiment

2.1. Materials

Sodium alginate (SA, $C_6H_7O_6Na$, AR), polyethyleneimine (PEI, MW 70,000 Da, AR), polyvinyl alcohol (PVA, MW 75,000 Da, hydrolyzation: 99%, AR), sodium diethyldithiocarbamate trihydrate ($C_5H_{16}NNaO_3S_2$, copper reagent, AR), and copper chloride dihydrate ($CuCl_2{\cdot}2H_2O$, AR) were purchased from Sinopharm Chemical Reagent Co. (Shanghai, China). The specifications of raw materials are all AR. All the reagents were used as received, without further purification.

2.2. Solution Preparation

For the experiment, a 97.00 g solution of sodium alginate was prepared by dissolving 3.00 g of powder in deionized water and stirring for 8 h. Similarly, a 3.00 g PEI solution was prepared in 97.00 g of deionized water and sonicated for 15 min. For the PVA solution, 5.00 g of PVA particles were soaked in 95.00 g of deionized water for 4 h at room temperature, followed by heating and stirring at 90 °C for 6 h to achieve complete dissolution. All solutions were labeled and stored accordingly.

In the preparation of hybrid electrospinning solutions, SA and PVA were mixed at a 1:3 mass ratio, while PEI and PVA were mixed at a 1:4 ratio. Both mixtures were thoroughly vortexed, shaken, and sonicated to remove air bubbles. Cu^{2+} solutions were prepared by dissolving $CuCl_2$ in deionized water to achieve concentrations ranging from 2 mg/L to 10 mg/L. Additionally, a 1 g/L solution of sodium diethylthiocarbamate trihydrate was prepared. All solutions were accurately prepared to facilitate further experimentation.

2.3. Preparation of SA/PEI/PVA Multilayer Composite Nanofiber Membrane

The experiment involved the electrospinning of two mixed liquids, designated as No. 1 and No. 2. Initially, the liquids were drawn into syringes and spun under controlled conditions. The process began by wrapping a circle of tin foil around the receiving drum to aid in the removal of the nanofiber membrane. A zero wire connected the voltage device to the drum, and the ground wire was accessed. After verifying the connections, the experiment commenced. Using the No. 1 syringe, the liquid was injected at a rate of 4–10 μL/min using an automatic liquid supply pump. The needle-to-drum distance was maintained at 5–15 cm, and the voltage was set to 17–20 kV. After injecting 0.5 mL, spinning was paused to switch to the No. 2 syringe. This syringe was used to inject liquid at a rate of 8–12 μL/min under the same distance and voltage settings. This process was repeated, alternating between the two syringes, until a total volume of more than 10 mL was spun. Once complete, the nanofiber film was carefully removed from the tin foil, sealed in a bag, labeled, and stored in a desiccator for future use.

2.4. Cu^{2+} Filtration

The setup of the filtration apparatus begins with assembling the necessary components: a top cover, a funnel filter cup, a sand core filter head, and an Erlenmeyer flask. These are arranged vertically from top to bottom and held securely in place by stainless steel clamps to maintain stability throughout the process. The lower section of the sand core funnel is attached to a conduit that directs the filtrate straight into the Erlenmeyer flask.

To prepare the filter membrane, a nanofiber membrane is first sized by tracing and cutting out a circle that matches the diameter of the sand core funnel using a compass and scissors. This membrane is then sandwiched between two filter papers of the same size to prevent any damage from the filtration hardware. This assembly is then placed on the sand core funnel. The setup is completed by connecting a through-hole beaker to the sand core funnel with a sealing film and a clamp to ensure a tight, leak-free connection.

Before initiating the filtration, 100 mL of a pre-prepared 8 mg/L Cu^{2+} solution is added to the through-hole beaker. After securing the top cap, the system is left to allow the solution to gradually pass through the nanofiber membrane into the Erlenmeyer flask below. Once filtration is complete, the filtrate is collected and prepared for UV analysis. For

assessing the membrane's reusability and durability, several filtration cycles are performed. Each cycle uses 80 mL of the 8 mg/L Cu^{2+} solution, and after each use, the nanofiber membrane is carefully sealed and stored. The cycles are conducted every 8 h, totaling six repetitions. The filtrate from each cycle is gathered and marked for subsequent evaluation and testing. This procedure not only evaluates the membrane's filtration capabilities but also tests its stability and reliability for repeated use.

2.5. Membrane Characterization

The morphology of the multilayer composite nanofiber membranes was observed using a field emission scanning electron microscope (NovaNano450, FEI, Hillsboro, OR, USA). The membrane surface was analyzed for elements using an X-ray spectrometer (Octane Plus, EDAX, Mahwah, NJ, USA). The nanofiber membranes, SA solid powder, and PVA solid powder were characterized on an X-ray diffraction analyzer with a scanning range of 10–80° (2θ). The prepared SA/PEI/PVA multilayer composite nanofiber membranes were placed in a standard thermogravimetric analyzer (STA449F3, NETZSCH, Selb, Germany) with an atmosphere of air, a ramp rate of 10 K/min, and a test temperature range of 20–300 °C. The nanofiber membranes were then analyzed in a standard thermogravimetric analyzer (STA449F3, NETZSCH, Selb, Germany). The prepared SA/PEI/PVA multilayer composite nanofiber membrane samples were oven-dried, ground, and pressed with potassium bromide, and then scanned and analyzed with a Fourier Transform infrared absorption spectrometer (FTIR, Nicolet iS10, Thermo Fisher Scientific, Waltham, MA, USA) in the wavelength range of 4000–500 cm^{-1}. The 10 mg/L, 8 mg/L, 6 mg/L, 4 mg/L, and 2 mg/L Cu^{2+} solutions configured were detected with a UV-visible spectrophotometer, and the absorbance–concentration relationship was analyzed by the five-point fitting method. Six cuvettes were prepared and 3 mL of 10 mg/L, 8 mg/L, 6 mg/L, 4 mg/L, and 2 mg/L Cu^{2+} solution were measured in a cylinder and added into five quartz cuvettes, and the sixth quartz cuvette was filled with 3 mL of deionized water to serve as the baseline and control. Two drops of copper reagent configured were added to the quartz cuvettes with Cu^{2+} solution and scanned and analyzed by UV-visible spectrophotometer to plot absorbance versus concentration for the next step of filtration detection. The assay method for the filtrate to be tested is the same as above, which is to take 3 mL of filtrate and add two drops of copper reagent. The detection method for recirculation filtration is the same as above.

3. Results and Discussion

3.1. SEM Analysis of SA/PEI/PVA Multilayer Composite Nanofiber Membrane

To observe the microstructure of SA/PEI/PVA multilayer composite nanofibrous membranes, we carried out SEM analysis, of which representative ones were selected for analysis, and fiber diameter analysis was carried out for the ones with better morphology, as shown in Figure 1. Through repeated experiments and by adjusting different spinning process parameters, we obtained a more complete set of spinning parameters. As shown in Figure 1, the adopted SA:PEI:PVA ratios were 3:5:9 and 1:2:6, respectively. Comparison of the results in Figure 1A,B showed that the fiber morphology obtained from spinning was more obvious and of higher quality under these parameters. By decreasing the jetting speed of the spinning solution, the blobs on the nanofibers were significantly reduced. In addition, by slightly increasing the spinning voltage, as shown in Figure 1C, we observed a significant improvement in the spinning effect, with enhanced filamentation of the spun nanofiber film and no more blobs on the fiber surface. These adjustments optimized the spinning process and improved the quality of the nanofibrous membranes.

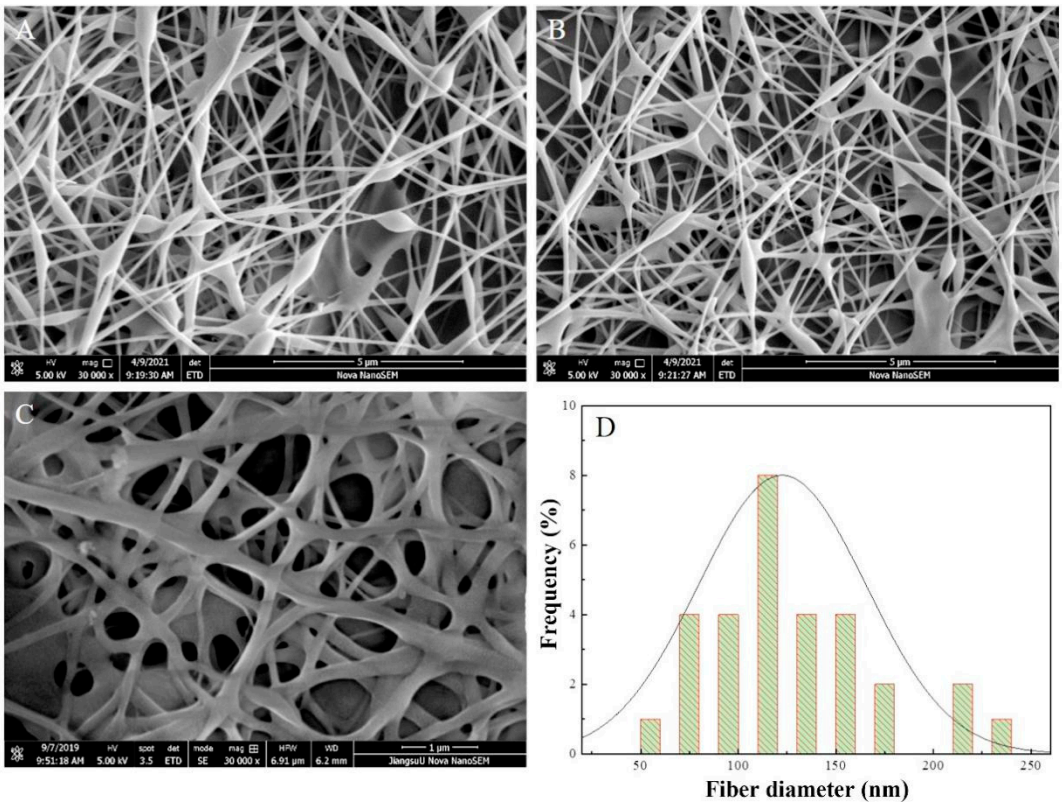

Figure 1. SEM images of the multilayer composite nanofiber membranes with different mass ratios of SA:PEI:PVA. (**A**) 3:5:9, 19 kV, 8 cm; (**B**) 1:2:6, 19 kV, 8 cm; (**C**) 1:2:6, 19.5 kV, 8 cm. (**D**) Composite nanofiber membrane fiber diameter distribution histograms.

The fiber diameter measurements in Figure 1C were analyzed, and the results are shown in Figure 1D. The analysis results show that the fiber diameter of SA/PEI/PVA multilayer composite nanofiber membrane spun with the data of Figure 1C was concentrated at 70–160 nm, and the average diameter reached 112.5 nm. The fiber diameter of the spun multilayer composite nanofiber membrane was more uniform, and the fiber diameter achieved the expected effect.

By keeping the distance, spinning liquid mixing ratio, temperature, and humidity unchanged and by adjusting the voltage and jetting speed, a slight increase in the voltage was obtained, as well as a decrease in the jetting speed in this system. For the spinning process, the appearance of small spheres on the nanofibers, as well as nanofiber homogeneity, was changed more favorably.

3.2. EDS Analysis of SA/PEI/PVA Multilayer Composite Nanofiber Membranes

To assess the adsorption of heavy metal ions by SA/PEI/PVA multilayer composite nanofibrous membranes before and after filtration, we conducted EDS scans on the membranes used before and after filtration and recorded the elemental content. The originated membranes and those preserved after filtration with their elemental distributions are shown in Figures 2 and 3, and the elemental data are listed in Tables 1 and 2, respectively. In Figure 2, green markers indicate carbon elements (A), red markers indicate nitrogen elements (B), and blue markers indicate oxygen elements (C). The EDS results indicate that the surface elements of the SA/PEI/PVA multilayer composite nanofibrous membranes are consistent with the elements found in the raw materials SA, PEI, and PVA, with no other impurities detected. Figure 3 presents the EDS scan results of the membranes after filtration, where green, red, and blue markers represent carbon, nitrogen, and oxygen elements, respectively, like Figure 2. The yellow markers (D) indicate the presence of copper elements, showing that the post-filtration nanofibrous membranes retained the elements

from the raw materials and successfully adsorbed Cu^{2+} from the solution. The uniform distribution of copper elements (as shown in Figure 3D) confirms the uniform distribution of Cu^{2+} adsorbing functional groups on the membrane, further validating its effectiveness in adsorbing heavy metal ions.

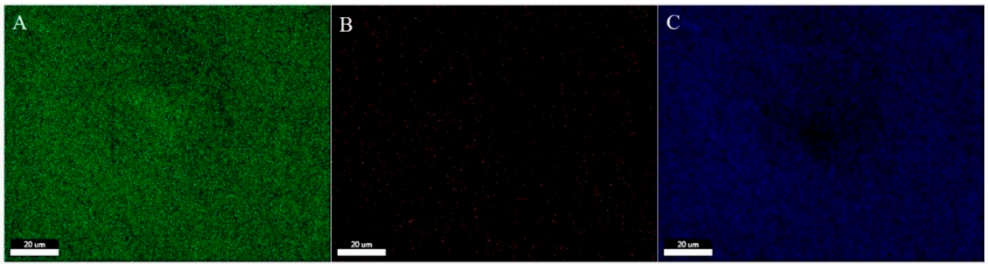

Figure 2. Elemental map of SA/PEI/PVA multilayer composite nanofiber membranes before filtration. (**A**) C; (**B**) N; (**C**) O.

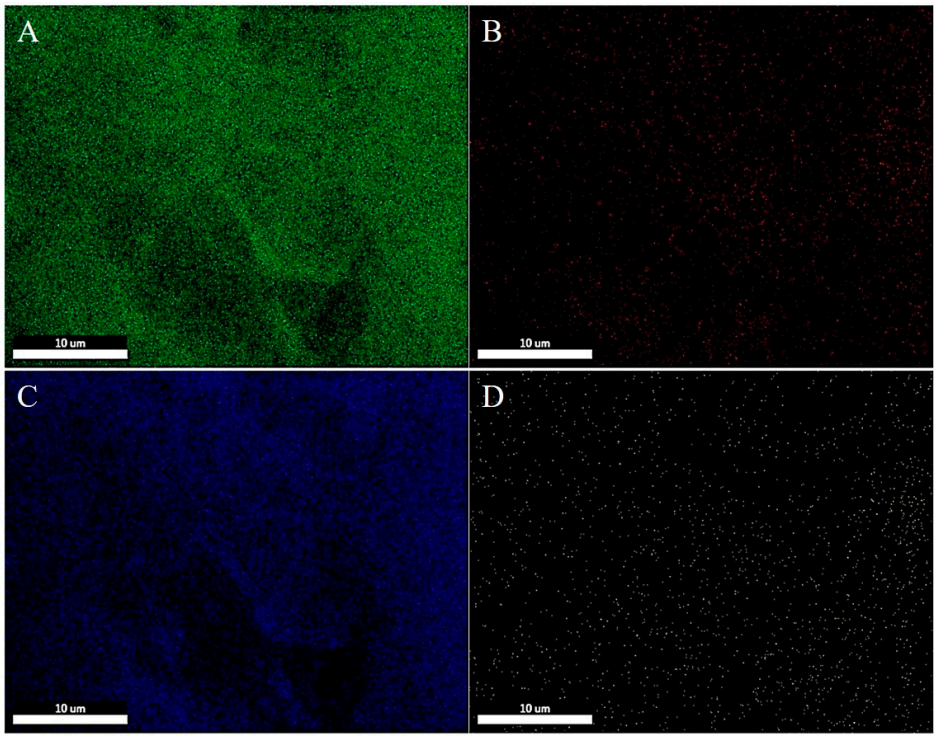

Figure 3. EDS elemental maps of SA/PEI/PVA multilayer composite nanofiber membrane filtration after filtration. (**A**) C; (**B**) N; (**C**) O; (**D**) Cu.

Table 1. Element percentage table for SA/PEI/PVA multilayer composite nanofiber membrane filtration pre-pointing EDS.

	Wt.%	
C	**N**	**O**
63	1	35

Table 2. Element percentage table for SA/PEI/PVA multilayer composite nanofiber membrane filtration after punching EDS.

	Wt.%		
C	**N**	**O**	**Cu**
75	1	23	1

The EDS analysis revealed that the concentration of O before filtration was significantly higher than that after filtration. This observation can be attributed to the high selective adsorption capacity of sodium alginate fiber molecules for Cu^{2+}. Following adsorption, the O atoms on the carboxyl group (-COOH) bound to Cu^{2+} were no longer detectable or exhibited reduced signal intensity, resulting in a notable difference in concentration. This evidence supports the adsorption of sodium alginate from the side. Furthermore, the formation of a three-dimensional reticulated gel structure upon binding with Cu^{2+} may result in alterations to the distribution and accessibility of O atoms. A portion of the O atoms may become buried within the gel structure, preventing their detection and resulting in a low concentration.

The EDS analysis revealed that the concentration of C before filtration was considerably lower than that observed after filtration. This may be attributed to the observed change in the molecular structure of sodium alginate fiber molecules following the adsorption of Cu^{2+}. Such alterations may result in the molecular chains undergoing stretching, cross-linking, or twisting, which could lead to significant changes in the distribution and exposure of certain carbon atoms, potentially influencing the EDS results. Furthermore, the combination of Cu^{2+} with carboxyl functional groups may result in the rearrangement or exposure of the C atoms in the molecular chain, which in turn leads to an enhanced detection signal.

Additionally, Cu^{2+} may interact with specific functional groups in the fiber molecules, altering the reaction of these functional groups in the EDS and leading to changes in concentration.

3.3. XRD Analysis of SA/PEI/PVA Multilayer Composite Nanofiber Membrane

The crystalline properties of SA/PEI/PVA multilayer composite nanofiber membranes were investigated using XRD. Figure 4 shows the XRD diffraction patterns of pure SA, pure PVA, and multilayer composite nanofiber membranes, respectively. The analysis reveals that pure SA had limited crystallization capability, while pure PVA exhibited excellent crystallization properties. The multilayer composite nanofiber membrane, created by incorporating SA and PEI, integrated the characteristics of all three materials. It retained the crystalline properties of PVA and displayed the amorphous peak of SA at 19.8°, indicating a uniform blend of the three components within the multilayer composite nanofiber membrane.

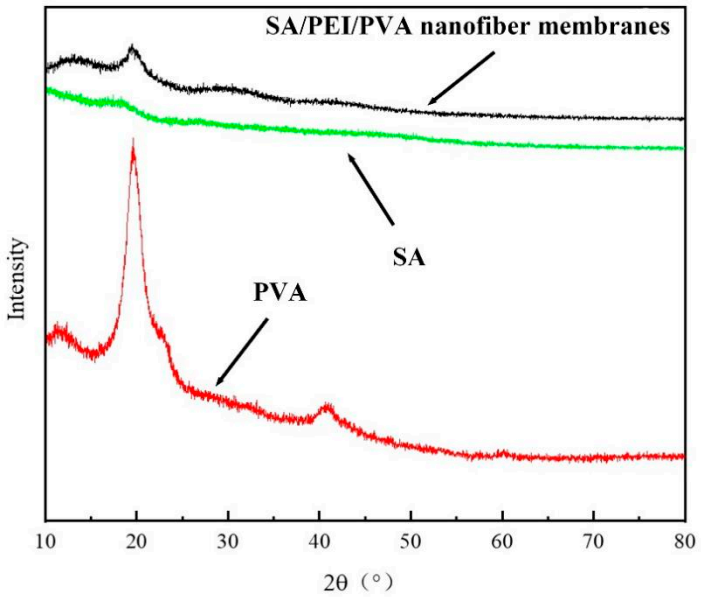

Figure 4. XRD test analysis images of pure SA, pure PVA, and multilayer composite nanofiber membranes.

3.4. FTIR Analysis of SA/PEI/PVA Multilayer Composite Nanofiber Membrane

To analyze and verify the effective functional groups of Cu^{2+} adsorbed on SA/PEI/PVA multilayer composite nanofiber membranes, we performed FTIR analysis, and the results

are shown in Figure 5. The absorption peaks at 1106.5 cm^{-1} and 1384.7 cm^{-1} represent the stretching and bending vibration of the carboxyl group (-COOH). Compared with the pre-filtration, the absorption peaks at 1106.5 cm^{-1} and 1384.7 cm^{-1} disappeared from the membrane after filtration, which also verifies that the sodium alginate embedding mechanism described in the previous section was used to adsorb and remove the Cu from the solution. The absorption peaks at 1647 cm^{-1} represent iminos (-NH_2) and C-H in alkanes, and the absorption peaks on the membrane after filtration were significantly reduced compared with those before filtration, which proves that the iminos were also consumed during the filtration of Cu^{2+}, which is related to the filtration of Cu^{2+}.

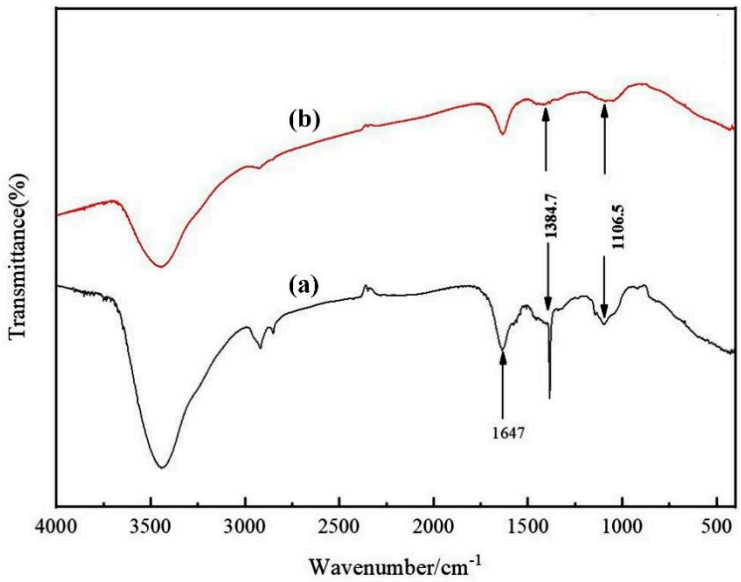

Figure 5. FTIR of nanofiber membrane before (**a**) and after (**b**) filtration.

3.5. TG Analysis of SA/PEI/PVA Multilayer Composite Nanofiber Membranes

In addition to the research basis of the microstructure, the structural performance of the prepared SA/PEI/PVA multilayer composite nanofiltration membranes was evaluated. Through TG analysis, the testing conditions were set to increase from room temperature to 300 °C with a temperature ramping rate of 10 K/min, which simulated a testing environment close to the actual filtration conditions. The results are demonstrated in Figure 6, where the nanofiber membrane gradually lost mass as the temperature increased, and this mass loss was mainly attributed to several key factors. First, at lower temperature intervals—room temperature to 100 degrees Celsius—the mass loss mainly stemmed from the evaporation of water adsorbed in the nanofiber membrane. Second, solvents that may have been left over from the preparation process evaporated during heating, also contributing to some of the mass reduction. With the further increase in temperature, the polymer chain segments also underwent pyrolysis and produced volatiles. However, pyrolysis of the polymer chain segments was not significant at room temperature, which is the conventional operating temperature for copper ion filtration. This indicates that the prepared multilayered composite nanofiber membranes had excellent thermal stability under this temperature condition. Therefore, it can be expected that the nanofiber membrane can maintain stable structure and performance during the copper ion filtration process, thus ensuring high filtration efficiency. This is of great significance for filtration operations in practical applications. Especially in the case of fluctuating ambient temperatures or localized heating during operation, the stability is more likely to ensure the consistency and reliability of the filtration effect.

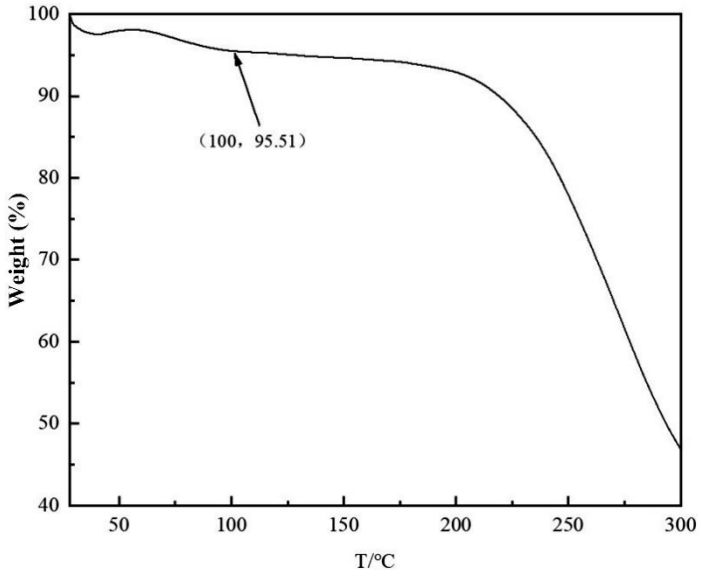

Figure 6. TG of SA/PEI/PVA multilayer composite nanofiber membrane.

3.6. Filtration Efficiency of Cu^{2+} via UV-Vis

To assess the filtration efficiency of SA/PEI/PVA multilayer composite nanofibers for Cu^{2+} ions, the filtrate was calculated and analyzed using UV-vis spectroscopy. This method measures the absorption of visible light by different concentrations of Cu^{2+}, where each solution correlates to a specific absorbance value. Since Cu^{2+} ions themselves do not absorb light, a copper reagent was added to enable light absorption. To maintain consistency across all test samples, an equal concentration and volume of copper reagent were added to each sample, ensuring uniformity in the quantity of reagent filtered. The results are presented in Figure 7, which illustrates the UV-vis spectroscopic analysis of the samples. Figure 7A displays the detection results for the standard concentration of Cu^{2+}, where the absorption peak of Cu^{2+} appeared around 450 nm. By analyzing the absorbance of Cu^{2+} in five different standard concentration gradients, we created the concentration–absorbance relationship curve shown in Figure 7B. This curve was constructed using the five-point method, achieving an R^2 value of $\geq$99%, which indicates a highly accurate correlation between concentration and absorbance. Using this relationship, the theoretical concentration of copper ions calculated for any given absorbance closely matched the actual concentration.

Through the relationship curve of concentration–absorbance obtained by UV-vis detection and analysis, we analyzed the filtrate by UV-vis detection and analysis, and the detection method was the same as that of the standard sample. The efficiency of filtration was calculated by analyzing the detection results after filtration and calculating the concentration of copper ions after filtration through the relationship curve in Figure 7B. The efficiency of filtration was calculated to be 87.3%, and the results are shown in Figure 7C. In addition, we also carried out repeated filtration experiments of Cu^{2+}, and the detection method of ion concentration after filtration was the same as that of the standard samples, and the results obtained from Figure 7B were used in the calculation of the filtrate concentration. In the cyclic filtration, the concentration of Cu^{2+} in each filtration was 8 mg/L, and the volume was 50 mL. Cyclic filtration was carried out six times, and the results obtained are shown in Figure 7D. The efficiency of the filtration was unchanged in the first four filtrations, and the adsorption effect had a significant decrease from the fifth time onward. One of the decreasing factors of the adsorption results could be that the adsorption capacity of the nanofiber membrane reached the limit, and the other one could be that the structure of the nanofiber membrane was damaged, which led to the decreasing adsorption effect.

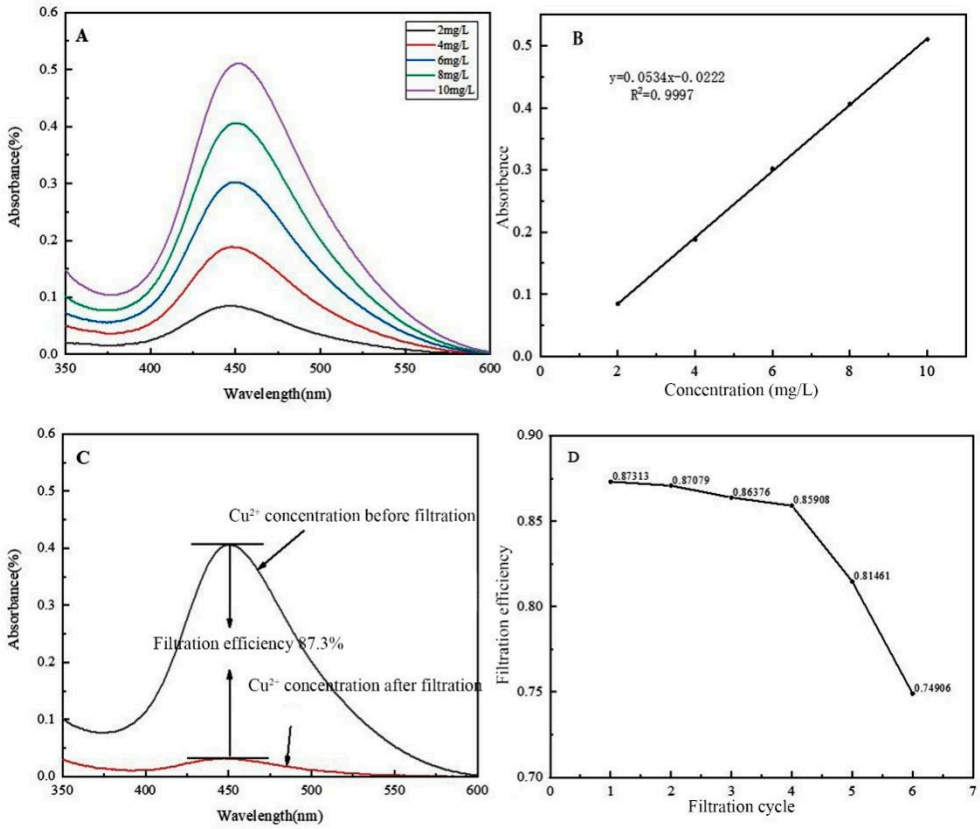

Figure 7. UV-vis detection results. (**A**) standard concentration Cu^{2+} detection results; (**B**) Cu^{2+} concentration versus absorbance; (**C**) Cu^{2+} filtration efficiency; (**D**) Cu^{2+} cyclic filtration efficiency.

4. Conclusions

In this study, SA/PEI/PVA multilayer composite nanofibrous membranes were prepared by electrostatic spinning technology, a series of multilayer composite nanofibrous membranes was prepared by adjusting the parameters of the spinning process, and their structures and properties were fundamentally characterized using analytical test methods such as SEM, FTIR, EDS, UV-vis, XRD, TG, and so on. The results show that the spinning process of the polymer solution could effectively change the microstructure of the nanofibers by reducing the injection speed and increasing the voltage so that the spun nanofiber membranes were more uniform and continuous. The prepared SA/PEI/PVA multilayer composite nanofiber membrane reached more than 85% adsorption efficiency of Cu(II) in a single instance, and its adsorption efficiency of Cu(II) could still be maintained at more than 80% when it was reused four times. The effective functional groups of carboxyl (-COOH) and imino (-NH_2) for Cu(II) adsorption on the prepared SA/PEI/PVA multilayer composite nanofiber membranes were analyzed by the FTIR results. This sustainable approach not only provides an efficient method for heavy metal removal but also utilizes biodegradable and non-toxic materials, aligning with environmental protection and resource conservation efforts. The reuse capability of the nanofibers further enhances their sustainability profile, reducing waste and promoting long-term application.

Author Contributions: Conceptualization, Z.Z. and S.W.; methodology, Z.Z.; validation, B.X. and Y.L.; formal analysis, L.C.; investigation, Y.L. and W.S.; data curation, C.X.; writing—original draft, B.X.; writing—review & editing, S.W.; supervision, S.W.; funding acquisition, S.W. All authors have read and agreed to the published version of the manuscript.

Funding: This work was supported by the National Natural Science Foundation of China (51808263).

Institutional Review Board Statement: Not applicable.

Informed Consent Statement: Not applicable.

Data Availability Statement: Data are contained within the article.

Conflicts of Interest: The authors declare no conflict of interest.

References

1. Jiang, E.H.; Song, N.; Zhang, X.X.; Yang, L.L.; Liu, C.B.; Dong, H.J. In-situ fabrication of Z-scheme $Bi_3O_4Cl/Bi_{12}O_{17}Cl_2$ heterostructure by facile pH control strategy to boost removal of various pollutants in water. *Chem. Eng. J.* **2020**, *388*, 13. [CrossRef]
2. Peng, J.Y.; Zhang, S.; Han, Y.Y.; Bate, B.; Ke, H.; Chen, Y.M. Soil heavy metal pollution of industrial legacies in China and health risk assessment. *Sci. Total Environ.* **2022**, *816*, 12. [CrossRef] [PubMed]
3. Wang, Z.; Luo, P.P.; Zha, X.B.; Xu, C.Y.; Kang, S.X.; Zhou, M.M.; Nover, D.; Wang, Y.H. Overview assessment of risk evaluation and treatment technologies for heavy metal pollution of water and soil. *J. Clean. Prod.* **2022**, *379*, 15. [CrossRef]
4. Zhu, B.; Shao, R.Q.; Li, N.; Min, C.Y.; Liu, S.K.; Xu, Z.W.; Qian, X.M.; Wang, L.J. Progress of cyclodextrin based-membranes in water treatment: Special 3D bowl-like structure to achieve excellent separation. *Chem. Eng. J.* **2022**, *449*, 21. [CrossRef]
5. Li, Z.; Yin, L.; Jiang, S.; Chen, L.; Sang, S.; Zhang, H. A photocatalytic degradation self-cleaning composite membrane for oil-water separation inspired by light-trapping effect of moth-eye. *J. Membr. Sci.* **2023**, *669*, 121337. [CrossRef]
6. Shi, W.; Xu, C.; Cai, J.; Wu, S. Advancements in material selection and application research for mixed matrix membranes in water treatment. *J. Environ. Chem. Eng.* **2023**, *11*, 111292. [CrossRef]
7. Wu, S.; Shi, W.; Cui, L.; Xu, C. Enhancing contaminant rejection efficiency with ZIF-8 molecular sieving in sustainable mixed matrix membranes. *Chem. Eng. J.* **2024**, *482*, 148954. [CrossRef]
8. Wang, Z.; Cui, Y.; Feng, Y.; Guan, L.; Dong, M.; Liu, Z.; Liu, L. A versatile Silk Fibroin based filtration membrane with enhanced mechanical property, disinfection and biodegradability. *Chem. Eng. J.* **2021**, *426*, 131947. [CrossRef]
9. Yuan, C.; Zhou, K.; Wang, Y.; Xie, Y.; Jing, W.; Xing, W. Enhanced micro-explosion to improve the yield of light oil in catalytic cracking of water-in-heavy oil emulsion prepared by continuous membrane emulsification. *Fuel* **2024**, *358*, 130122. [CrossRef]
10. Lu, Y.; Zhang, Y.; Zhang, K. Renewable biomass resources to access halogen- and phosphorus-free flame retardant thermosets with ultra-low heat release capacity. *Chem. Eng. J.* **2022**, *448*, 9. [CrossRef]
11. Yue, X.; Wang, Z.; Shi, H.; Wu, R.; Feng, Y.; Yuan, L.; Hou, S.; Song, X.; Liu, L. Silk fibroin-based piezoelectric nanofibrous scaffolds for rapid wound healing. *Biomater. Sci.* **2023**, *11*, 5232–5239. [CrossRef] [PubMed]
12. Wan, Y.; Liu, Z.-Y.; Song, P.; Zhang, X.-Q.; Song, J.-C.; Fu, Y.-J.; Yao, X.-H.; Wang, J.; Chen, T.; Zhang, D.-Y. Ionic liquid groups modified 3D porous cellulose microspheres for selective adsorption of AO7 dye. *J. Clean. Prod.* **2019**, *240*, 118201. [CrossRef]
13. Zhao, Y.-M.; Li, Y.; Ma, H.; He, R. Effects of ultrasonic-assisted pH shift treatment on physicochemical properties of electrospinning nanofibers made from rapeseed protein isolates. *Ultrason. Sonochem.* **2023**, *94*, 106336. [CrossRef] [PubMed]
14. Chen, Y.; Gu, B.; Li, Y.; Yang, D.; Qiu, F.; Zhang, T. Fabrication of MnO_2 nanowires@ Ag/cellulose laminated membranes with unidirectional liquid penetration for personal thermal management applications. *Ind. Eng. Chem. Res.* **2021**, *60*, 17980–17988. [CrossRef]
15. Yao, S.; Zhang, C.; Guo, R.; Majeed, A.; He, Y.; Wang, Y.; Shen, X.; Li, T.; Qin, S. CoS_2-decorated cobalt/nitrogen Co-doped carbon nanofiber networks as dual functional electrocatalysts for enhancing electrochemical redox kinetics in lithium–sulfur batteries. *ACS Sustain. Chem. Eng.* **2020**, *8*, 13600–13609. [CrossRef]
16. Yao, S.; Zhang, C.; Xie, F.; Xue, S.; Gao, K.; Guo, R.; Shen, X.; Li, T.; Qin, S. Hybrid membrane with SnS_2 nanoplates decorated nitrogen-doped carbon nanofibers as binder-free electrodes with ultrahigh sulfur loading for lithium sulfur batteries. *ACS Sustain. Chem. Eng.* **2020**, *8*, 2707–2715. [CrossRef]
17. Zhu, Y.; Wang, K.; Lu, J.; Pan, Z.; Rong, J.; Zhang, T.; Yang, D.; Pan, J.; Qiu, F. Teamed boronate affinity-functionalized Zn-MOF/PAN-derived molecularly imprinted hollow carbon electrospinning nanofibers for selective adsorption of shikimic acid. *ACS Appl. Mater. Interfaces* **2022**, *14*, 27294–27308. [CrossRef] [PubMed]
18. Li, Y.; Zhu, J.; Cheng, H.; Li, G.; Cho, H.; Jiang, M.; Gao, Q.; Zhang, X. Developments of advanced electrospinning techniques: A critical review. *Adv. Mater. Technol.* **2021**, *6*, 2100410. [CrossRef]
19. Rahmati, M.; Mills, D.K.; Urbanska, A.M.; Saeb, M.R.; Venugopal, J.R.; Ramakrishna, S.; Mozafari, M. Electrospinning for tissue engineering applications. *Prog. Mater. Sci.* **2021**, *117*, 100721. [CrossRef]
20. Luraghi, A.; Peri, F.; Moroni, L. Electrospinning for drug delivery applications: A review. *J. Control. Release* **2021**, *334*, 463–484. [CrossRef]
21. Wu, S.; Shi, W.; Li, K.; Cai, J.; Xu, C.; Gao, L.; Lu, J.; Ding, F. Chitosan-based hollow nanofiber membranes with polyvinylpyrrolidone and polyvinyl alcohol for efficient removal and filtration of organic dyes and heavy metals. *Int. J. Biol. Macromol.* **2023**, *239*, 124264. [CrossRef] [PubMed]
22. Li, X.; Chen, W.; Qian, Q.; Huang, H.; Chen, Y.; Wang, Z.; Chen, Q.; Yang, J.; Li, J.; Mai, Y.W. Electrospinning-based strategies for battery materials. *Adv. Energy Mater.* **2021**, *11*, 2000845. [CrossRef]
23. Xu, C.; Yue, C.; Yao, Y.; Yu, Y.; Li, L.; Liu, X. 3D cotton-like phase change fibers via electrospinning for thermal management of textile. *J. Energy Storage* **2024**, *84*, 110991. [CrossRef]

24. Yang, D.; Li, L.; Chen, B.; Shi, S.; Nie, J.; Ma, G. Functionalized chitosan electrospun nanofiber membranes for heavy-metal removal. *Polymer* **2019**, *163*, 74–85. [CrossRef]
25. Frent, O.D.; Vicas, L.G.; Duteanu, N.; Morgovan, C.M.; Jurca, T.; Pallag, A.; Muresan, M.E.; Filip, S.M.; Lucaciu, R.-L.; Marian, E. Sodium alginate—Natural microencapsulation material of polymeric microparticles. *Int. J. Mol. Sci.* **2022**, *23*, 12108. [CrossRef] [PubMed]
26. Shaikh, M.A.J.; Gupta, G.; Afzal, O.; Gupta, M.M.; Goyal, A.; Altamimi, A.S.A.; Alzarea, S.I.; Almalki, W.H.; Kazmi, I.; Negi, P. Sodium alginate-based drug delivery for diabetes management: A review. *Int. J. Biol. Macromol.* **2023**, *236*, 123986. [CrossRef] [PubMed]
27. Wei, Q.; Zhou, J.; An, Y.; Li, M.; Zhang, J.; Yang, S. Modification, 3D printing process and application of sodium alginate based hydrogels in soft tissue engineering: A review. *Int. J. Biol. Macromol.* **2023**, *232*, 123450. [CrossRef] [PubMed]
28. Wang, Q.; Li, L.; Tian, Y.; Kong, L.; Cai, G.; Zhang, H.; Zhang, J.; Zuo, W.; Wen, B. Shapeable amino-functionalized sodium alginate aerogel for high-performance adsorption of Cr (VI) and Cd (II): Experimental and theoretical investigations. *Chem. Eng. J.* **2022**, *446*, 137430. [CrossRef]
29. Yang, Y.; Yu, X.; Zhu, Y.; Zeng, Y.; Fang, C.; Liu, Y.; Hu, S.; Ge, Y.; Jiang, W. Preparation and application of a colorimetric film based on sodium alginate/sodium carboxymethyl cellulose incorporated with rose anthocyanins. *Food Chem.* **2022**, *393*, 133342. [CrossRef] [PubMed]
30. Verma, A.; Thakur, S.; Mamba, G.; Gupta, R.K.; Thakur, P.; Thakur, V.K. Graphite modified sodium alginate hydrogel composite for efficient removal of malachite green dye. *Int. J. Biol. Macromol.* **2020**, *148*, 1130–1139. [CrossRef]
31. Arafa, E.G.; Sabaa, M.W.; Mohamed, R.R.; Kamel, E.M.; Elzanaty, A.M.; Mahmoud, A.M.; Abdel-Gawad, O.F. Eco-friendly and biodegradable sodium alginate/quaternized chitosan hydrogel for controlled release of urea and its antimicrobial activity. *Carbohydr. Polym.* **2022**, *291*, 119555. [CrossRef] [PubMed]
32. Li, T.; Wei, H.; Zhang, Y.; Wan, T.; Cui, D.; Zhao, S.; Zhang, T.; Ji, Y.; Algadi, H.; Guo, Z. Sodium alginate reinforced polyacrylamide/xanthan gum double network ionic hydrogels for stress sensing and self-powered wearable device applications. *Carbohydr. Polym.* **2023**, *309*, 120678. [CrossRef] [PubMed]
33. Al-Araji, D.D.; Al-Ani, F.H.; Alsalhy, Q.F. Polyethyleneimine (PEI) grafted silica nanoparticles for polyethersulfone membranes modification and their outlooks for wastewater treatment—A review. *Int. J. Environ. Anal. Chem.* **2023**, *103*, 4752–4776. [CrossRef]
34. Dube, S.; Moutloali, R.; Malinga, S. Hyperbranched polyethyleneimine/multi-walled carbon nanotubes polyethersulfone membrane incorporated with Fe-Cu bimetallic nanoparticles for water treatment. *J. Environ. Chem. Eng.* **2020**, *8*, 103962. [CrossRef]
35. Shati, A.A.; Alfaifi, M.Y.; Elbehairi, S.E.I.; Olegovich, B.D.; Althomali, R.H.; Abdullaev, S.S.; Saleh, E.A.M.; Hussien, B.M.; Abid, M.K.; Alwave, M. Functionalization of porous silica with graphene oxide and polyethyleneimine, containing zinc copper ferrite nanoparticles for water treatment and antibacterial application. *Environ. Pollut.* **2024**, *348*, 123745. [CrossRef] [PubMed]
36. Xiang, J.; Li, H.; Hei, Y.; Tian, G.; Zhang, L.; Cheng, P.; Zhang, J.; Tang, N. Preparation of highly permeable electropositive nanofiltration membranes using quaternized polyethyleneimine for dye wastewater treatment. *J. Water Process Eng.* **2022**, *48*, 102831. [CrossRef]
37. Xiong, S.; Han, C.; Phommachanh, A.; Li, W.; Xu, S.; Wang, Y. High-performance loose nanofiltration membrane prepared with assembly of covalently cross-linked polyethyleneimine-based polyelectrolytes for textile wastewater treatment. *Sep. Purif. Technol.* **2021**, *274*, 119105. [CrossRef]
38. Gao, W.; Razanajatovo, M.R.; Song, Y.; Zhao, X.; Zhao, Z.; Peng, Q.; Jiao, T.; Liu, X.; Zhang, Q. Efficient heavy metal sequestration from water by Mussel-inspired polystyrene conjugated with polyethyleneimine (PEI). *Chem. Eng. J.* **2022**, *429*, 132599. [CrossRef]
39. Bucatariu, F.; Ghiorghita, C.-A.; Zaharia, M.-M.; Schwarz, S.; Simon, F.; Mihai, M. Removal and separation of heavy metal ions from multicomponent simulated waters using silica/polyethyleneimine composite microparticles. *ACS Appl. Mater. Interfaces* **2020**, *12*, 37585–37596. [CrossRef]
40. Tofighy, M.A.; Mohammadi, T. Divalent heavy metal ions removal from contaminated water using positively charged membrane prepared from a new carbon nanomaterial and HPEI. *Chem. Eng. J.* **2020**, *388*, 124192. [CrossRef]